Supplementary Information

Integrating redox-electrodialysis and electrosorption for the removal of ultra-short- to long-chain PFAS

Nayeong Kim[1], Johannes Elbert[1], Ekaterina Shchukina[1], and Xiao Su[1]*

[1]Department of Chemical and Biomolecular Engineering, University of Illinois Urbana-Champaign, IL 61801, United States

Corresponding Author
*E-mail: x2su@illinois.edu

Table of Contents

SI 1. Concentrations of ultra-short-chain PFAS in various source waters

Table 1. Survey of ultra-short-chain PFAS in various source waters.

	Source water	Detected conc. (ppb)	Detected conc. (μM)	Region	Ref.
TFA	Groundwater from a rock shelter	14.00	0.1228	Sweden	[1]
	Groundwater	11.00	0.0965	Germany	[2]
	Surface water	17.00	0.1491	Germany	[2]
	Rainwater	2.400	0.0211	Delaware	[3]
		1.550	0.0136	Switzerland	[3]
	River water	10.00	0.0877	Germany	[4]
		22.00	0.1930	Bavaria	[5]
		140.0	1.2281	Germany	[5]
	Beer	51.00	0.4474	New Zealand	[6]
	Drinking water	1.105	0.0097	Netherlands	[7]
	Wastewater from electronic fabrication facilities	1.571	0.0138	Electronic Fabrication Facilities	[8]
		4.133	0.0363		[8]
		15.28	0.1340		[8]
	Effluents of wastewater treatment plants	206.0	1.8070	Switzerland	[9]
PFPrA	effluent water from a rock shelter	53.00	0.3232	Sweden	[1]
	Surface water	1.400	0.0085	China	[10]
		2.000	0.0122	China	[10]
	Wastewater from electronic fabrication facilities	1.125	0.0069	Electronic Fabrication Facilities	[8]
		4.184	0.0255		[8]

SI 2. Material synthesis and characterization

Calculation of terpolymer ratios

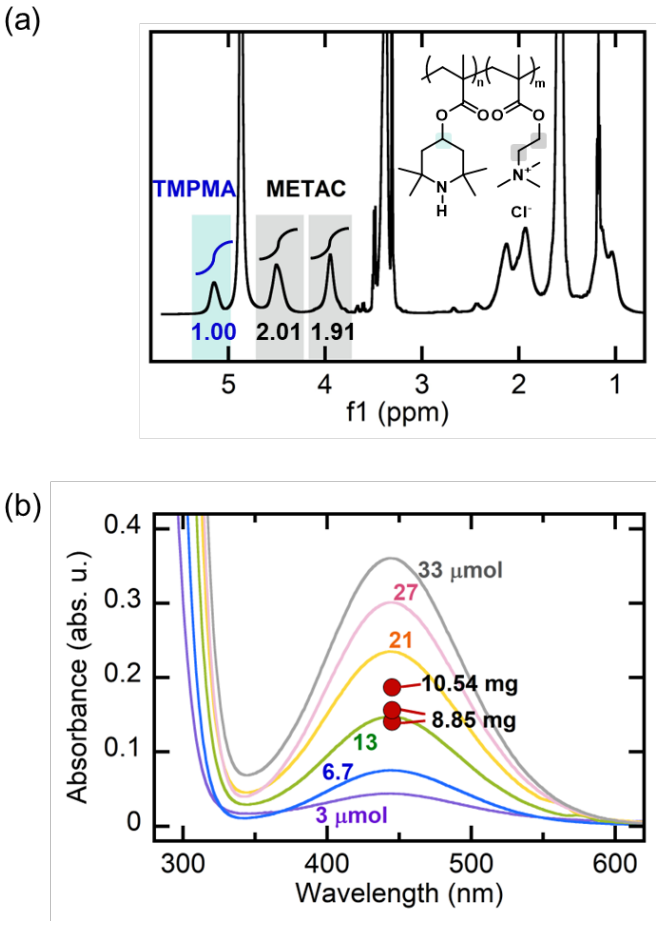

Figure 1: (a) ^{1}H-NMR spectrum of P(TMPMA-*co*-METAC) (500 MHz, dMeOH) and (b) UV-vis spectra of TEMPO reference (3-33 µM) and P(TMA-*co*-TMPMA-*co*-METAC) to calculate terpolymer ratios.

Polymer characterizations

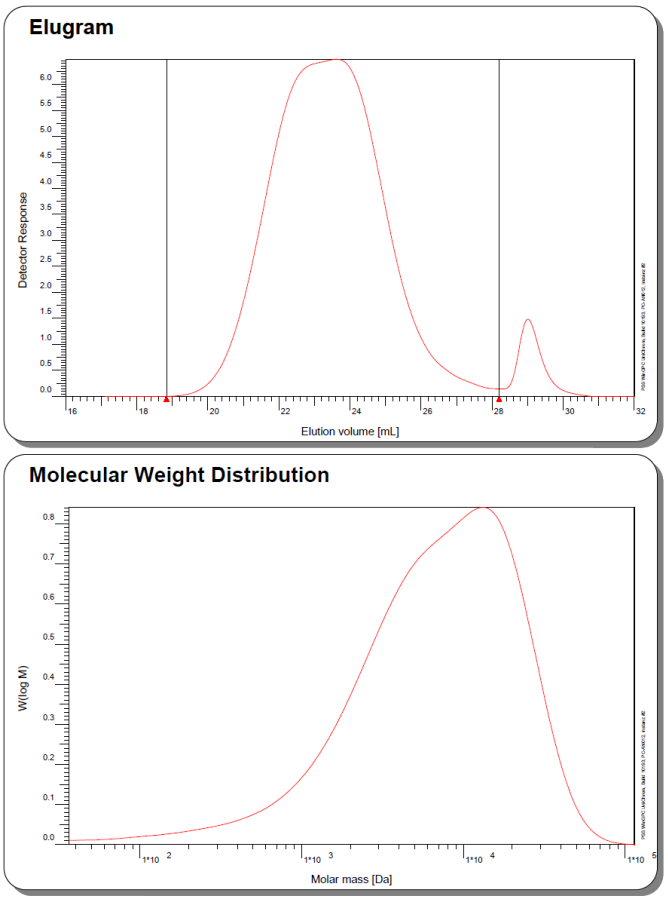

Figure 2: GPC results for P(TMA$_{33}$-*co*-TMPMA$_{17}$-*co*-METAC$_{50}$): (a) Elugram and (b) molecular weight distribution. The curve was integrated from 18.84 mL to 28.19 mL. GPC was performed with respect to the poly(2-vinylpyridine) standard using the column of PSS NOVEMA Max in 0.1 M NaCl and 0.1 vol% TFA with 50 µL injection volume and at a flow rate of 1 mL min^{-1}.

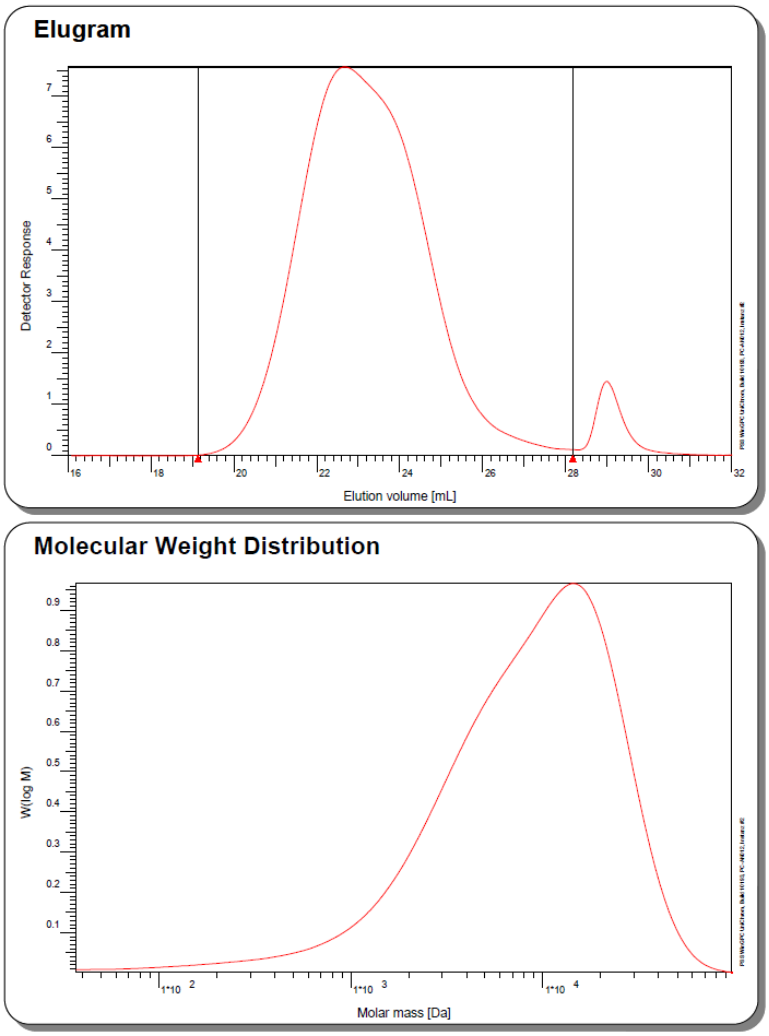

Figure 3: GPC results for recycled P(TMA$_{33}$-*co*-TMPMA$_{17}$-*co*-METAC$_{50}$) via dialysis method: (a) Elugram and (b) molecular weight distribution. The curve was integrated from 19.14 mL to 28.17 mL. GPC was performed with respect to the poly(2-vinylpyridine) standard using the column of PSS NOVEMA Max in 0.1 M NaCl and 0.1 vol% TFA with 50 µL injection volume and at a flow rate of 1 mL min^{-1}.

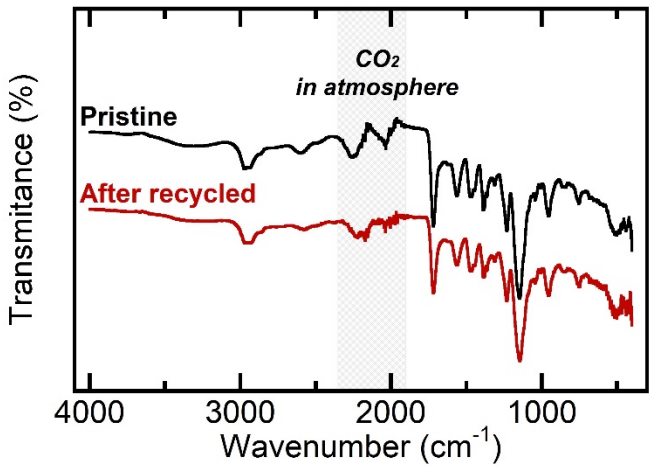

Figure 4: FTIR spectra of pristine and recycled P(TMA$_{33}$-*co*-TMPMA$_{17}$-*co*-METAC$_{50}$). There are no significant variations in the spectrum, indicating that the redox-copolymer retains functional groups like N-H (2800-3000 cm^{-1}), C=O (1720 cm^{-1}), N-O (1550 cm^{-1}), and C-N (1150 cm^{-1}).

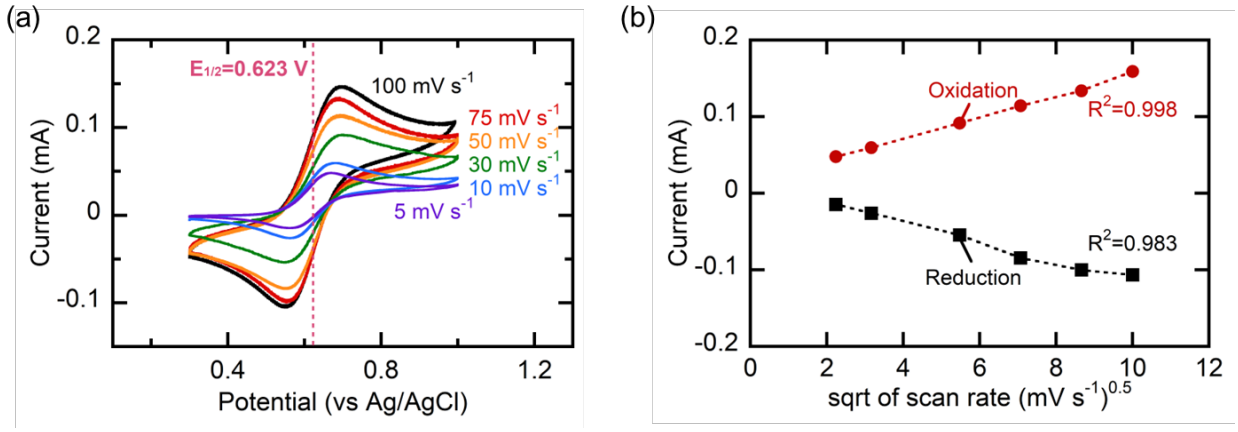

Figure 5: (a) Cyclic voltammograms and (b) Randles-Sevcik plot of recycled P(TMA$_{33}$-*co*-TMPMA$_{17}$-*co*-METAC$_{50}$) at different scan rates (5, 10, 30, 50, 75, 100 mV s^{-1}).

Table 2. Summary of polymer sizes and $E_{1/2}$ for pristine and after the recycle.

Polymer	Mn (g mol^{-1})	Mw (g mol^{-1})	Đ	$E_{1/2}$[a] [V]
Pristine	2260	10900	4.83	0.628
Recycled	2920	12200	4.17	0.623

[a)] Analyzed by GPC in H_2O with 0.1 M NaCl + 0.1% trifluoroacetic acid and poly(2-vinylpyridine) calibration; [b)] Determined by CV (vs. Ag/AgCl in 3 NaCl) with 30 mM P(TMA$_{33}$-*co*-TMPMA$_{17}$-*co*-METAC$_{50}$) and 100 mM NaCl.

Activated-carbon clothes characterizations

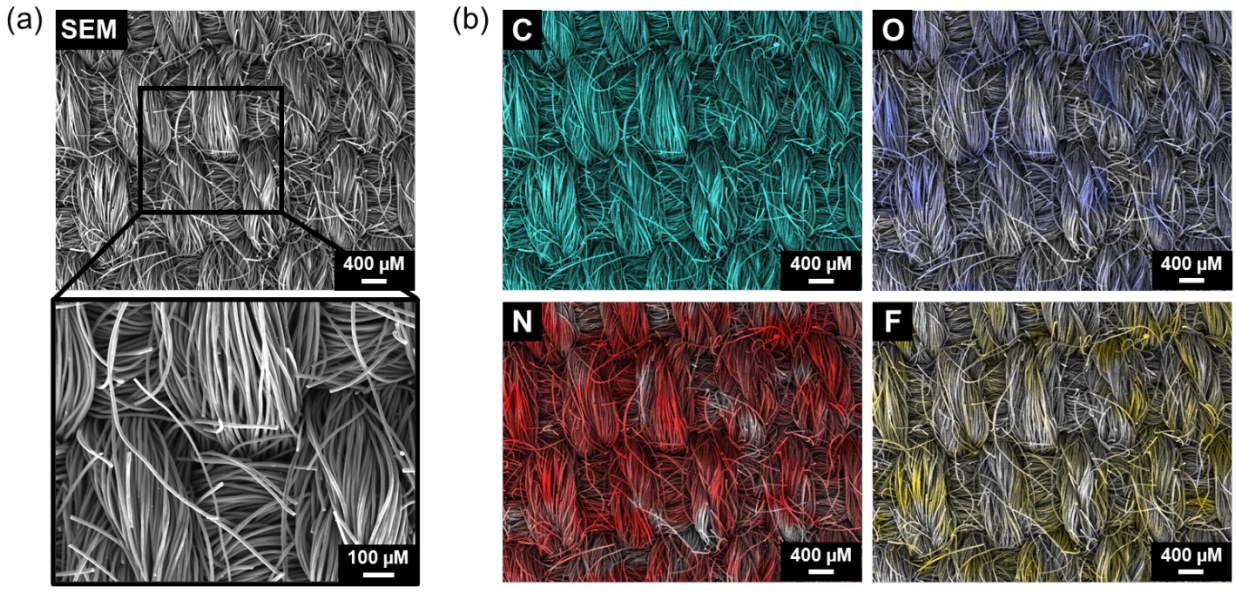

Figure 6: High-resolution (a) SEM images and (b) EDS mapping of the activated-carbon clothes (ACC). ACC predominantly comprises carbon, accompanied by trace amounts of nitrogen, oxygen, and fluoride. The presence of nitrogen and oxygen is likely attributed to functional groups like amine and OH, while fluoride may originate from the binder. The fabric is made of long carbon fibers with a diameter ranging from 11 to 15 µm.

Table 3. The composition of the activated-carbon clothes analyzed by the CHN and halide analysis.

Element	wt %
Carbon	97.72
Hydrogen	0.71
Nitrogen	0.39
Fluoride	0.03

Polymer binding affinity towards TFA and PFHxA

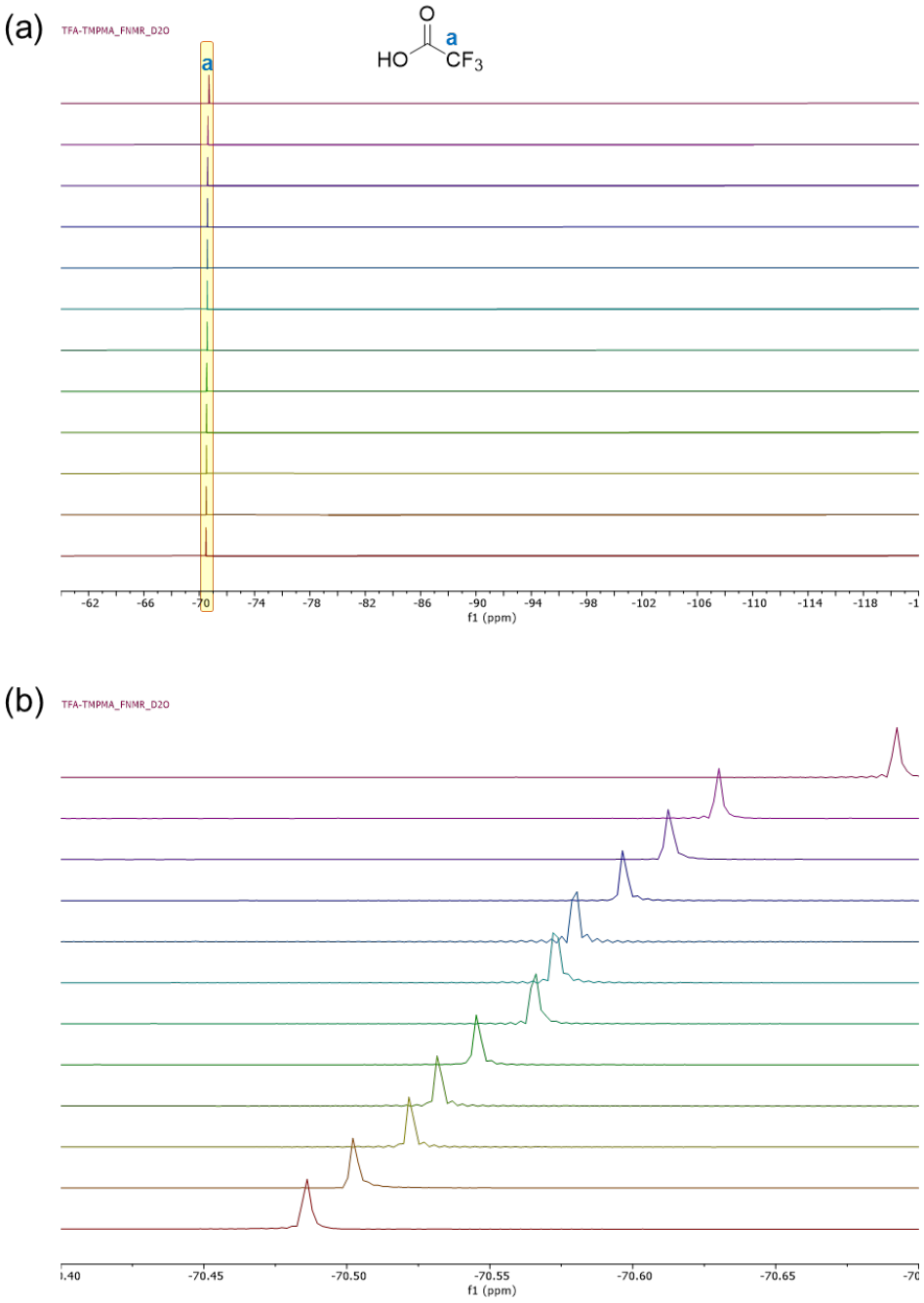

Figure 7: ^{19}F-NMR spectra (600 MHz, D_2O) of TMPMA titration in 20 mM TFA solution: (a) full spectrum range (-60 to -122 ppm) and (b) fluoride peak shift at Ca with 0, 0.1, 0.2, 0.3, 0.4, 0.5, 0.6, 0.7, 0.8, 0.9, 1.0, and 2.0 equivalents (from the bottom to top plots) of TMPMA (-70.4 to -70.7 ppm).

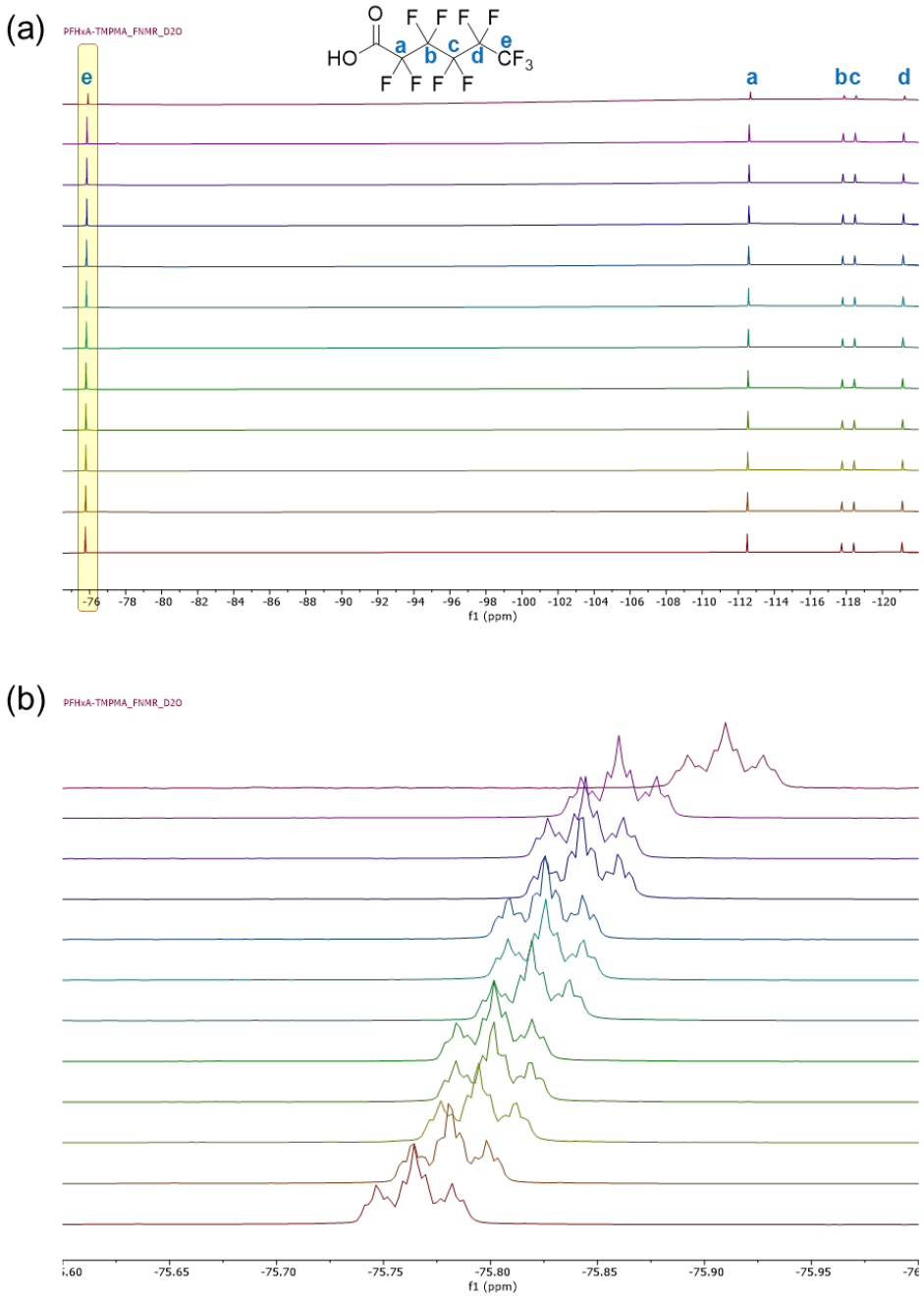

Figure 8: ^{19}F-NMR spectra (600 MHz, D_2O) of TMPMA titration in 20 mM PFHxA solution: (a) full spectrum range (-74.5 to -122 ppm) and (b) fluoride peak shift at Ce with 0, 0.1, 0.2, 0.3, 0.4, 0.5, 0.6, 0.7, 0.8, 0.9, 1.0, and 2.0 equivalents (from the bottom to top plots) of TMPMA (-75.6 to -76 ppm).

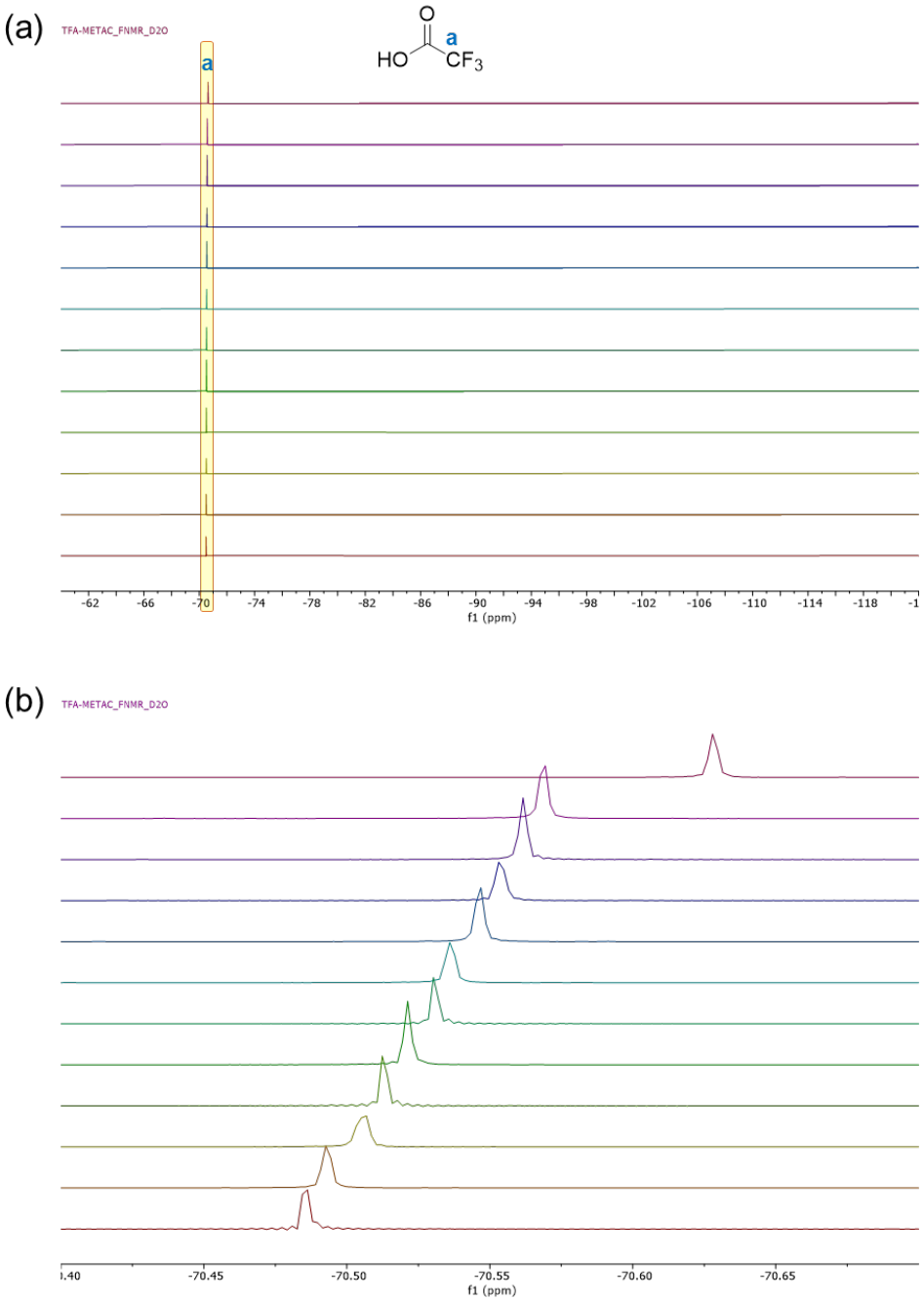

Figure 9: ^{19}F-NMR spectra (600 MHz, D_2O) of METAC titration in 20 mM TFA solution: (a) full spectrum range (-60 to -122 ppm) and (b) fluoride peak shift at Ca with 0, 0.1, 0.2, 0.3, 0.4, 0.5, 0.6, 0.7, 0.8, 0.9, 1.0, and 2.0 equivalents (from the bottom to top plots) of METAC (-70.4 to -70.7 ppm).

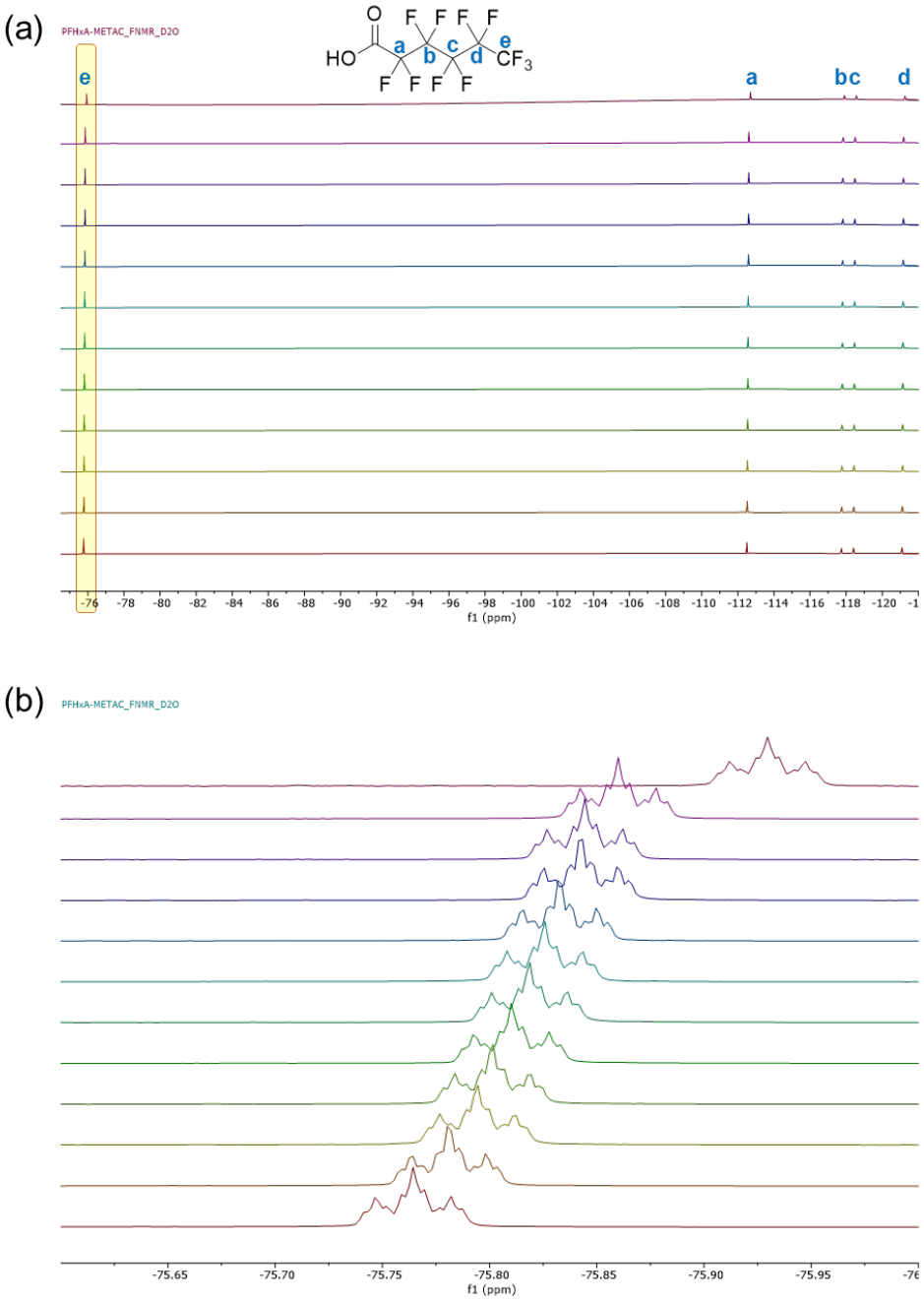

Figure 10: ^{19}F-NMR spectra (600 MHz, D_2O) of METAC titration in 20 mM PFHxA solution: (a) full spectrum range (-74.5 to -122 ppm) and (b) fluoride peak shift at Ce with 0, 0.1, 0.2, 0.3, 0.4, 0.5, 0.6, 0.7, 0.8, 0.9, 1.0, and 2.0 equivalents (from the bottom to top plots) of METAC (-75.6 to -76 ppm).

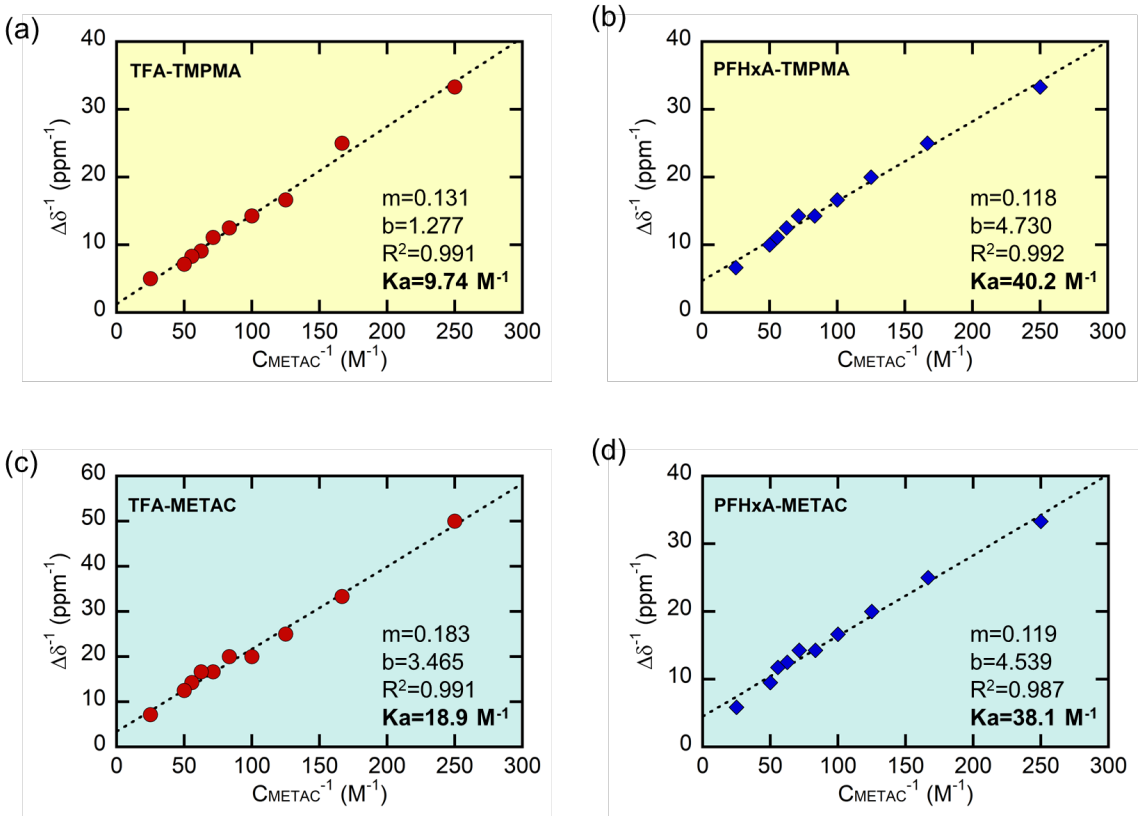

Figure 11: Benesi-Hildebrand plots and calculated binding constants (K_a) for (a) TFA and (b) PFHxA at different TMA concentrations, and for (a) TFA and (b) PFHxA at different METAC concentrations, calculated using the ^{19}F-NMR titration method.

SI 3. Examination of membrane fouling

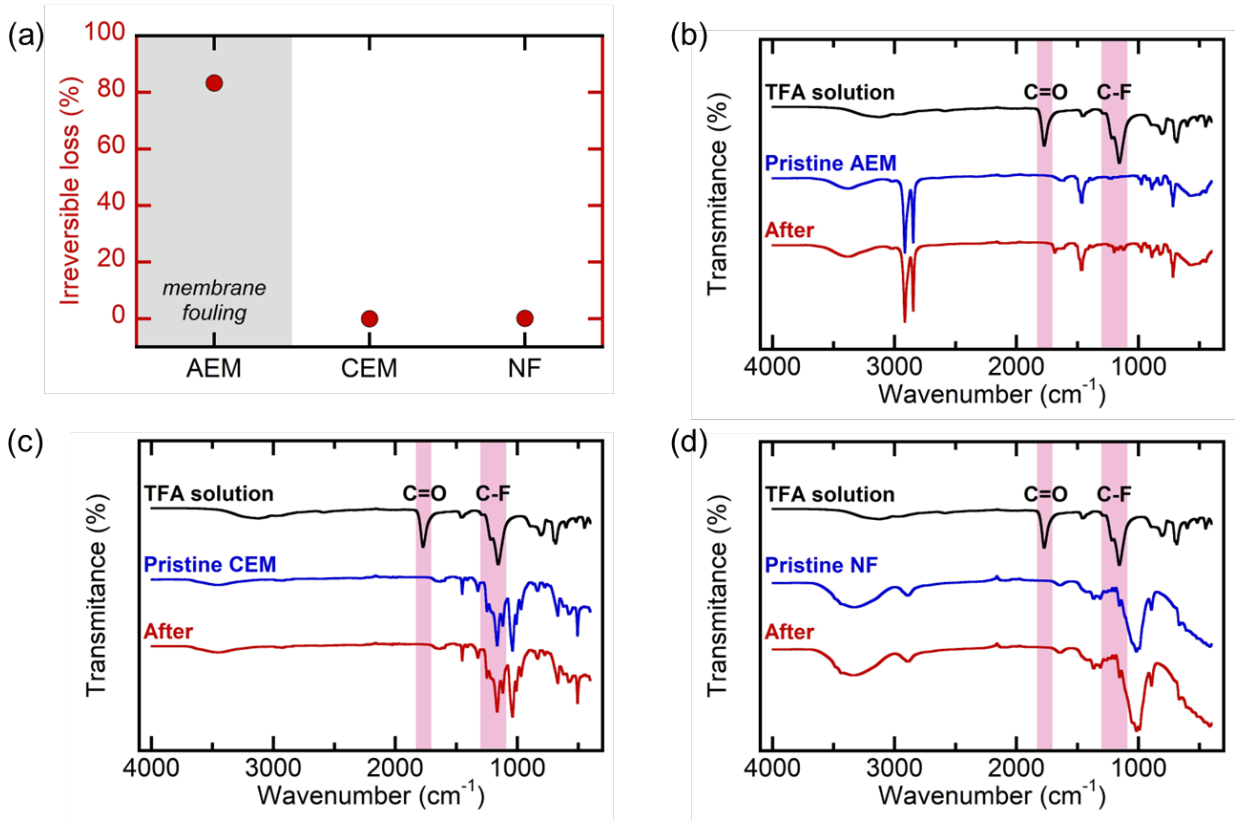

Figure 12: Membrane fouling test in the presence of 1 mM TFA. (a) The irreversible loss (%) of TFA after 24-hour immersion of AEM, CEM, and NF (2.0 × 2.0 cm^2). FTIR spectra of TFA solution, pristine, and after membrane fouling test for (b) AEM, (c) CEM, and (d) NF, showing the notable C=O and C-F peak formations on AEM. Figure 12a was generated with two replicates, and the average values along with their standard deviations were plotted.

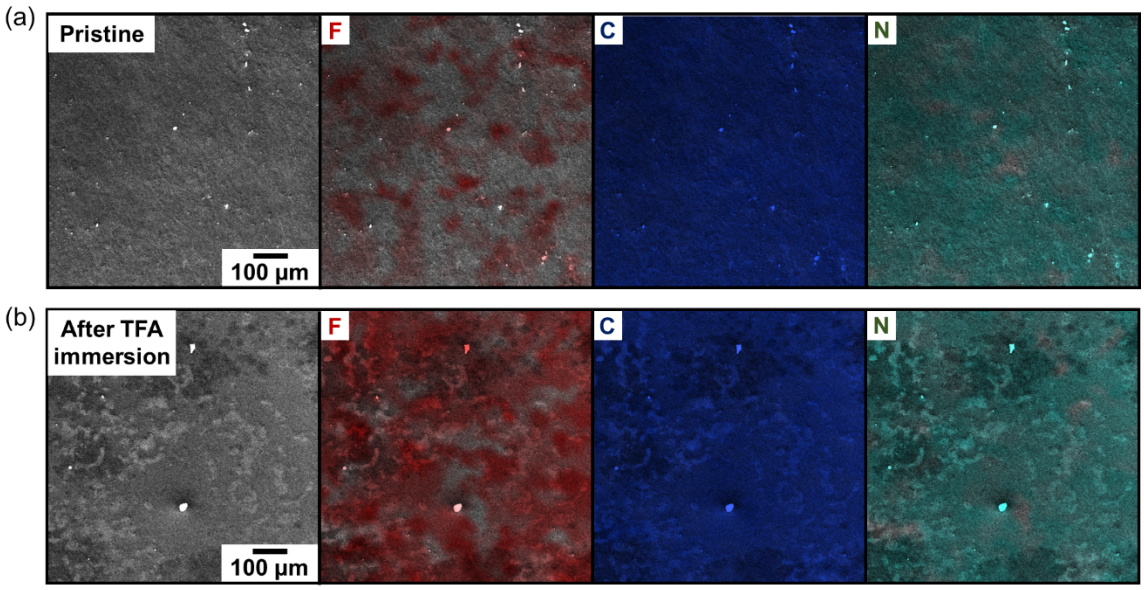

Figure 13: SEM images and EDS mappings (F, C, N) for (a) pristine AEM and (b) after a fouling test with a 2.0 × 2.0 cm^2 membrane immersed in 1 mM TFA and 10 mM NaCl for 24 hours. Note the distinct fluoride presence and the rougher, non-uniform surface in the SEM image after immersion in the TFA solution, indicating changes in surface morphology and the formation of aggregates.

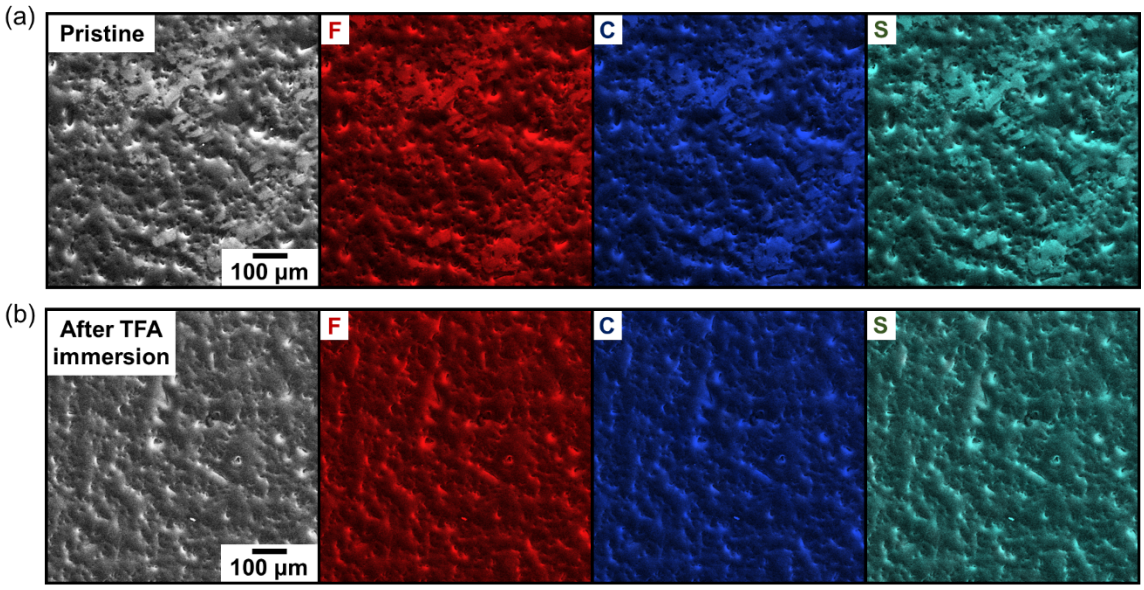

Figure 14: SEM images and EDS mappings (F, C, S) for (a) pristine CEM and (b) after a fouling test with a 2.0 × 2.0 cm^2 membrane immersed in 1 mM TFA and 10 mM NaCl for 24 hours. Due to the presence of binder contents, comparing the changes in fluoride contents after the membrane fouling test is challenging. Nevertheless, the lack of significant changes in concentrations (**Figure 12a**) and the absence of C=O bond formation (**Figure 12c**) in the FTIR spectrum indicates that no membrane fouling occurred on the CEM.

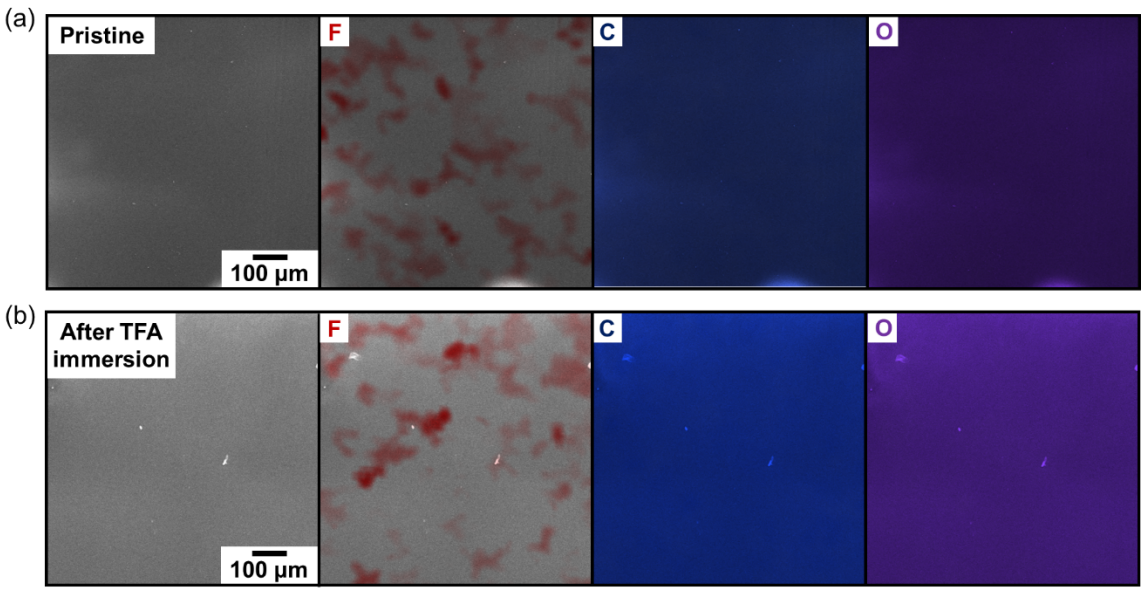

Figure 15: SEM images and EDS mappings (F, C, O) for (a) pristine NF and (b) after a fouling test with a 2.0 × 2.0 cm^2 membrane immersed in 1 mM TFA and 10 mM NaCl for 24 hours, indicate that no membrane fouling occurred on the NF.

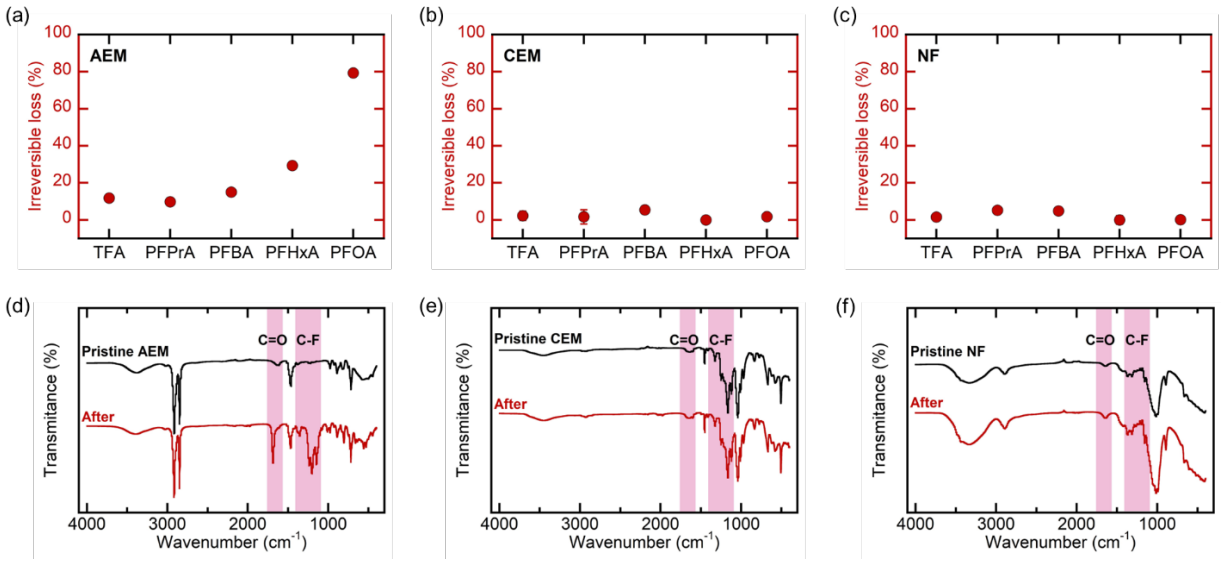

Figure 16: The irreversible loss (%) of PFAS contents after 24-hour immersion of (a) AEM, (b) CEM, and (c) NF (2.0 × 2.0 cm^2) in 1 mM TFA, PFPrA, PFBA, PFHxA, and PFOA. FTIR spectra of pristine and after membrane fouling test for (d) AEM, (e) CEM, and (f) NF, showing the notable C=O and C-F peak formations on AEM. Figures 16a-c were generated with two replicates, and the average values along with their standard deviations were plotted.

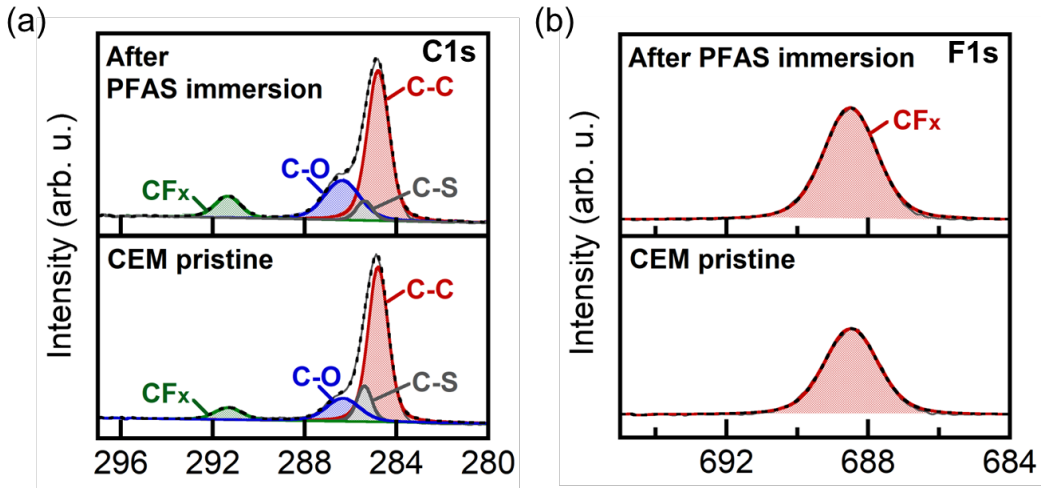

Figure 17: XPS spectra of (a) C1s and (b) F1s for CEM (2.0 × 2.0 cm^2) after 24-hour immersion of membranes in 1 mM TFA, PFPrA, PFBA, PFHxA, and PFOA.

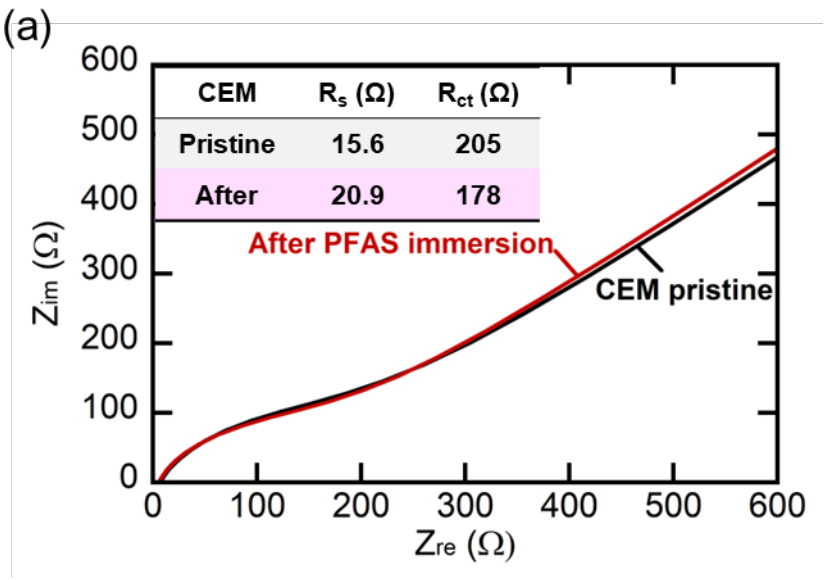

Figure 18: Nyquist plots of pristine CEM and after PFAS immersion. Membranes (2.0 × 2.0 cm^2) were immersed for 24 hours in 1 mM TFA, PFPrA, PFBA, PFHxA, and PFOA. R_s and R_{ct} correspond to system and charge-transfer resistances, respectively, and were calculated based on the equivalent circuit of R(Q(RW)). The inset table displays the values for system resistance (R_s) and charge transfer resistance (R_{ct}).

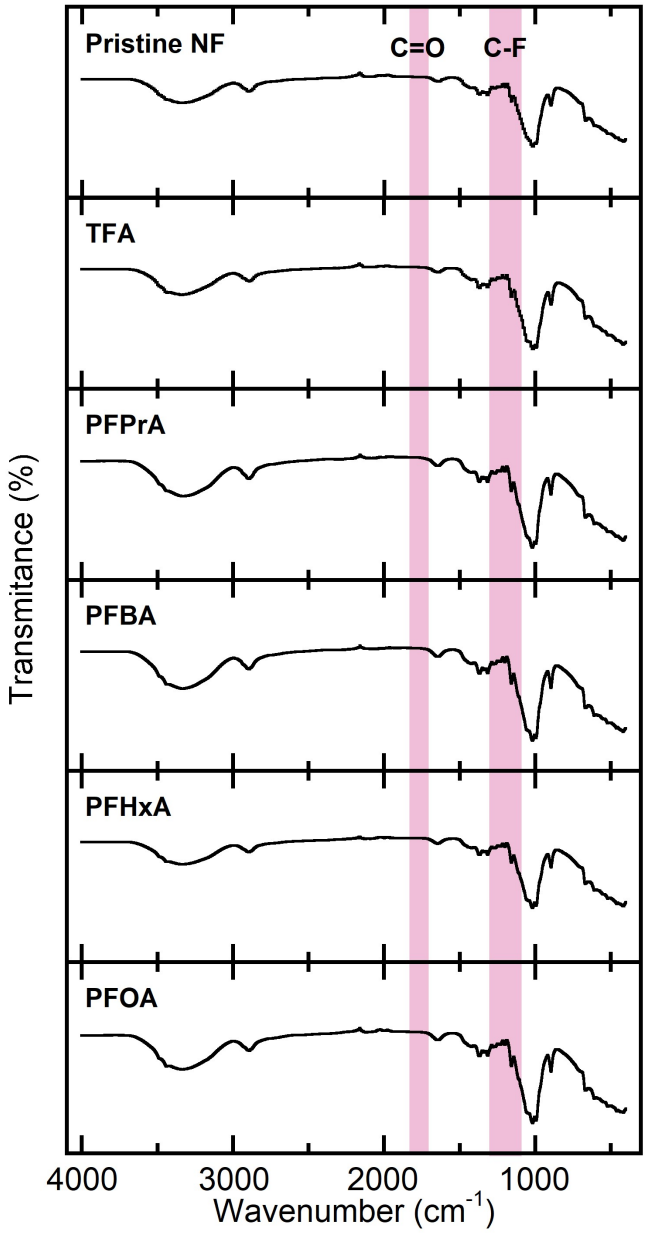

Figure 19: The fouling test involved immersing the NF (2.0 × 2.0 cm^2) in 1 mM of TFA (C2), PFPrA (C3), PFBA (C4), PFHxA (C6), and PFOA (C8) for 24 h, validating the absence of irreversible interactions between a wide range of PFAS and NF.

SI 4. Performance of redox-polymer ED for the removal of ultra-short chain PFAS

Evaluation of PFAS removal and desalination performance

The assessment of both PFAS removal and desalination performance involved evaluating various metrics, including removal percentage, energy consumption, and upconcentration percentage. The removal percentage, calculated using Equation 1, was used for both PFAS removal and desalination.

$$Removal\ percentage\ (\%) = {C_i - C_f}/{C_i} \quad \text{(Equation 1)}$$

, where C_i and C_f are initial and final concentrations of target species, respectively.

Then the energy consumption was calculated with respect to either PFAS removal (Equation 2) or both desalination and PFAS removal (Equation 3). Given that both PFAS removal and desalination were happening simultaneously in our system, we mostly used energy consumption with respect to both desalination and PFAS removal.

$$Energy\ consumption\ (kJ/mol_{PFAS}) = {V \int Idt}/{PFAS\ removal} \quad \text{(Equation 2)}$$

$$Energy\ consumption\ (kJ/(mol_{NaCl} + mol_{PFAS})) = {V \int Idt}/{(salt\ removal + PFAS\ removal)} \quad \text{(Equation 3)}$$

, V (V) represents the operating voltage, while I (A) denotes the current flowing within the system. The salt removal and PFAS removal were calculated by the concentration changes in the feed channel multiplied by the volume of the feed channel.

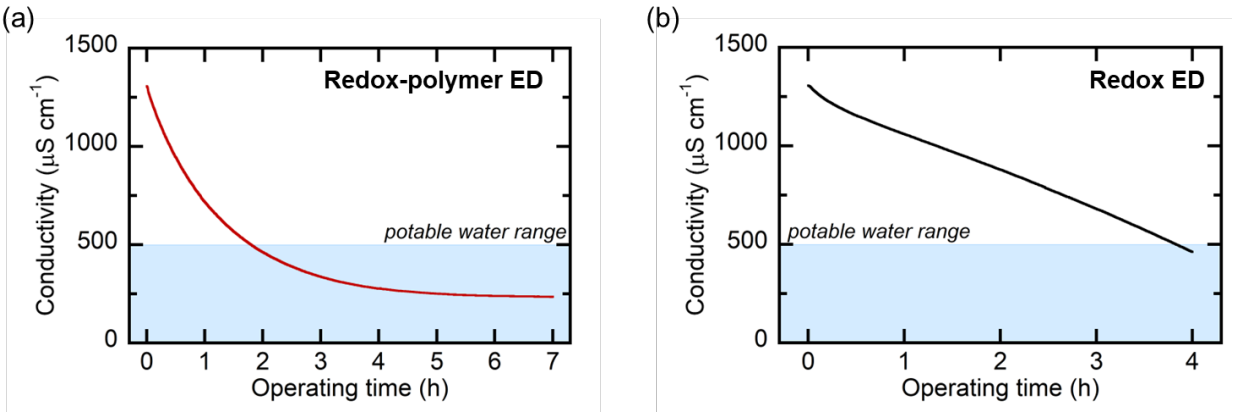

Figure 20: Conductivity profiles for the removal of 1 mM TFA with 10 mM NaCl using (a) redox-polymer ED and (b) redox ED.

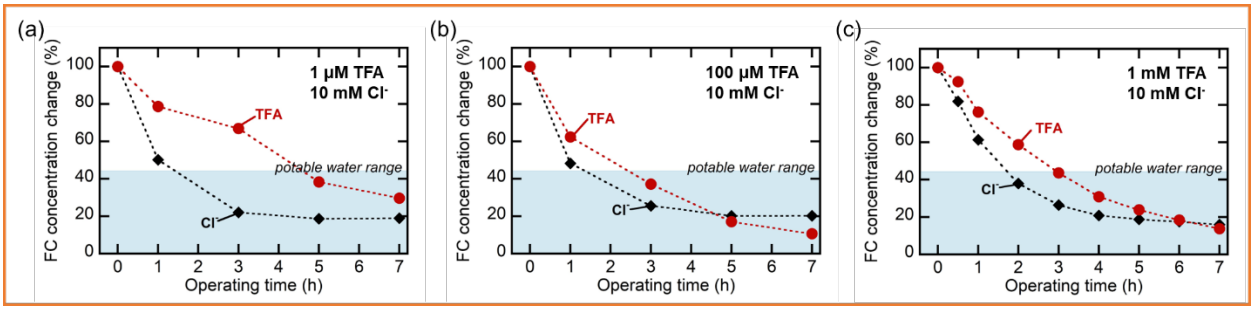

Figure 21: FC concentration changes for chloride and TFA in the presence of (a) 1 µM, (b) 100 µM, and 1 mM TFA with 10 mM Cl^-. The figure was generated with two replicates, and the average values along with their standard deviations were plotted.

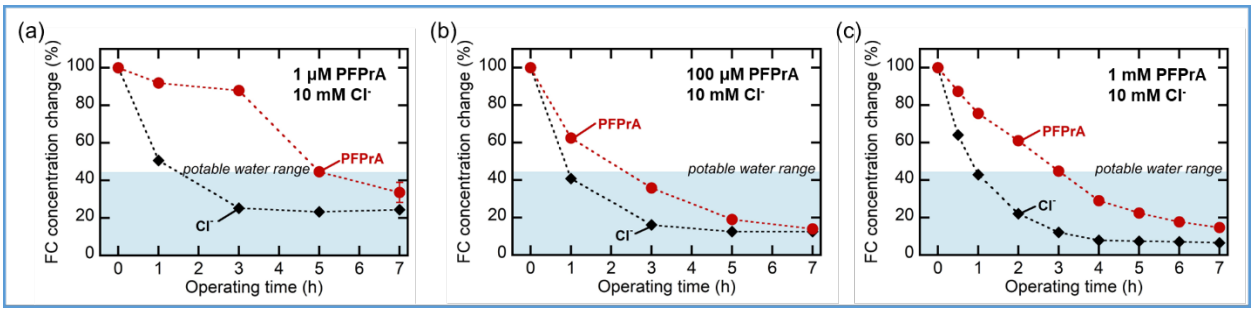

Figure 22: FC concentration changes for chloride and PFPrA in the presence of (a) 1 µM, (b) 100 µM, and 1 mM PFPrA with 10 mM Cl^-. The figure was generated with two replicates, and the average values along with their standard deviations were plotted.

SI 5. Single-process of ultra-short to long-chain PFAS removal

Performance comparison of PFAS removal and desalination between redox-polymer ED and conventional ED with NFs

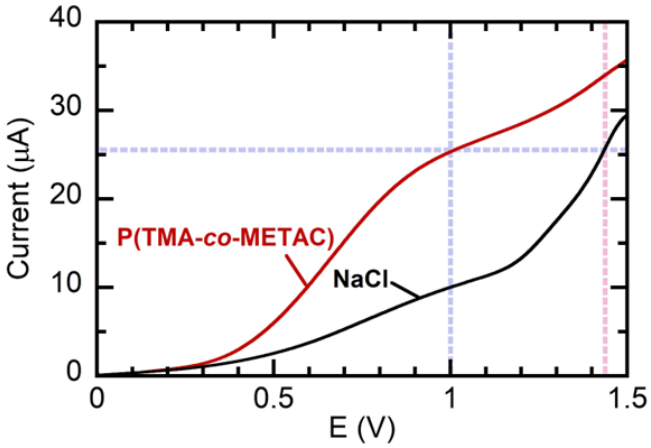

Figure 23. Linear sweep voltammetry (LSV) of the NF-enabled redox-ED system and conventional ED system with 30 mM NaCl to determine the operating voltage for the conventional ED system. The voltage at which the current matched that of the oxidation reaction of 30 mM P(TMA$_{33}$-*co*-TMPMA$_{17}$-*co*-METAC$_{50}$) at 1.0 V was 1.42 V. This identified voltage was applied as the operating voltage for conducting a control experiment using a conventional ED system.

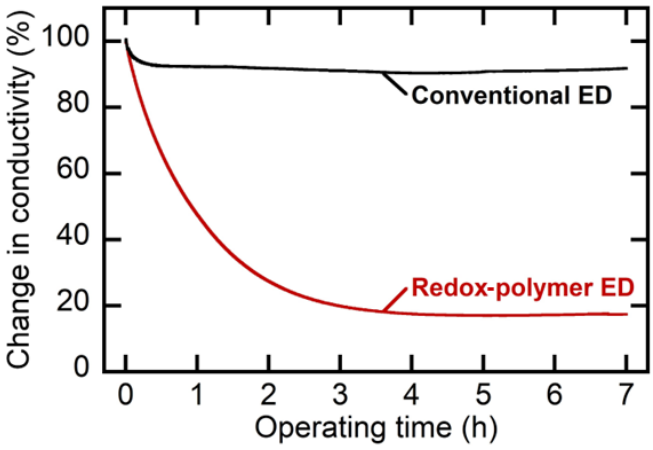

Figure 24. Changes in conductivity (%) for the redox-polymer ED with NF and conventional ED with NF for treating ultra-short to long-chain PFAS in tandem with desalination.

Examination of the mechanism of PFAS removal in the redox-polymer ED system

To achieve a thorough mechanistic understanding of PFAS removal in the redox-polymer ED, we examined the distribution of chloride and PFAS within the RC, AC, and FC (**Figure 25**). To distinguish between migration and electrosorption mechanisms clearly, we increased the initial concentration of PFAS and employed an equimolar concentration (2 mM) of chloride and PFAS as a feed channel. Chloride and PFAS concentrations for each compartment were assessed using IC and LC-MS, respectively. We analyzed the distribution of chloride and different chain lengths of PFAS in different components (e.g., FC, AC, RC, electrodes) based on the mass balance. Percent distribution was determined by dividing the concentrations in each component by the initial concentration in the feed channel.

In the presence of TFA and PFBA, over 80% of TFA was treated with minimal electrosorption, and less than 20% of treated PFBA was electrosorbed (**Figure 25a**). Similar PFAS removal and even lower electrosorption were observed for TFA and PFBA was observed when PFHxA and PFOA were added to the feed solution (**Figures 25b** and **c**). The result underlines that PFAS with chain lengths ≤C4 are mainly removed through migration, while PFAS with chain lengths ≥C6 are treated via electrosorption. Furthermore, 99% of chloride was desalinated throughout the experiments, highlighting the exceptional desalination capability of redox-polymer ED.

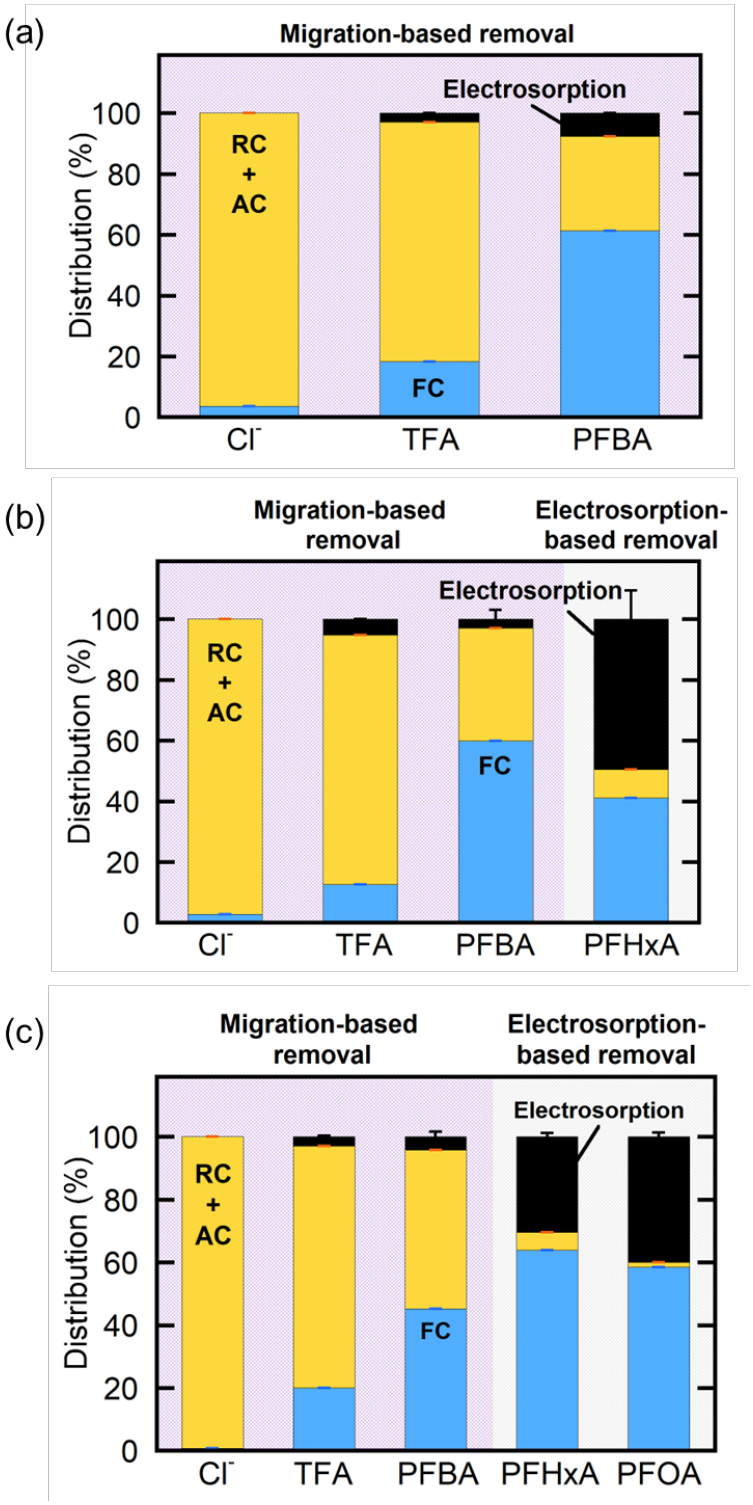

Figure 25. Distribution of chloride (Cl^-) and various PFAS species after 7-hour operation of redox-polymer ED systems in the feed solution containing (a) 2 mM Cl^-, TFA, and PFBA, (b) 2 mM Cl^-, TFA, PFBA, and PFHxA, and (c) 2 mM Cl^-, TFA, PFBA, PFHxA, and PFOA. The figure was generated with two replicates, and the average values along with their standard deviations were plotted.

SI 6. Coupling redox-polymer ED with electrochemical defluorination

Table 4. Summary of PFAS removal performance across various state-of-the-art technologies.

Removal techniques	Materials	Target PFAS	$C_{PFAS,i}$ (mM)	Removal performance	Ref
Adsorption	GAC, F400	PFOA	0.04-0.36	0.270 mmol/g, 0.193 mM, 0.1 g[a,b]	11
		PFBS	0.05-0.50	0.329 mmol/g, 0.233 mM, 0.1 g[a,b]	11
	GAC, Bamboo	PFOA	0.05-0.6	1.03 mmol/g, 0.34 mM, 10 mg[a,b]	12
	Quaternary nitrogen-grafted carbon (AWNQ)	TFA	0.09-0.88	34 μmol/g, 0.027 mM, 20 mg[a,b]	13
Electro-sorption	Ferrocene-based polymer, PFPMAm	PFOA	0.10	0.169 mmol/g[b]	14
	Cobaltocenium-based polymer, PMAECoPF6	PFOA	0.10	0.217 mmol/g[b]	14
	Fluorinated redox polymer, P(A98F2)	PFHxA	0.10	2.74 mmol/g	15
	Fluorinated redox polymer, P(A39T53F8)	PFBA	0.10	0.922 mmol/g	15
	Surface defunctionalized activated carbon felt (DeACF)	TFA	1.75	0.263 mmol/g	16
Ion exchange	IRA 67	PFOA	0.29[b]	2.82 mmol/g	17
		PFHxA	0.1[b]	0.53 mmol/g	17
	IRA910	PFOA	0.50	3.47 mmol/g	18
		PFHxA	0.50	3.47 mmol/g	18
		PFBA	0.50	2.97 mmol/g	18
	Purolite A520E	PFOA	2.41	0.323 mmol/g	19
		PFBA	4.67	0.138 mmol/g	19
Membrane	NFG	PFOA	0.00024	55.6%	20
		PFHxA	0.00032	38.6%	20
		PFBA	0.00047	18.7%	20
	NF90	PFOA	0.00024	97.4%	20
		PFHxA	0.00032	99.6%	20
		PFBA	0.00047	86.0%	20
	NF270	PFOA	0.24	99%	21
		PFOA	0.24	92.2%	21
	BW30-2540	PFOA	0.02	99.9%[a]	22
	BW30-2540	PFBA	0.05	99.9%[a]	22
	NF90-2540	PFOA	0.02	99.8%[a]	22
	NF90-2540	PFBA	0.05	99.7%[a]	22
NF-enabled redox polymer ED	**Cellulose-based NF (1 kDa), P(TMA-*co*-TMPMA-*co*-METAC)**	**PFOA**	**0.01**	**94.4%**	**Figure 5**
		PFHxA	**0.01**	**90.1%**	
		PFBA	**0.01**	**88.8%**	
		PFPrA	**0.01**	**90.3%**	
		TFA	**0.001-1**	**72.8-89.3%**	**Figure 4**
		PFPrA	**0.001-1**	**57.6-86.1%**	

[a] Equilibrium maximum adsorption capacity, equilibrium PFAS concentrations in aqueous phase, and sorbent loading.
[b] Calculated or estimated from the provided data.

Table S5. The anion composition of wastewater samples.

Anion (mM)			
Cl^-	NO_3^-	SO_4^{2-}	HPO_4^{2-}
16.85	1.75	6.82	0.965

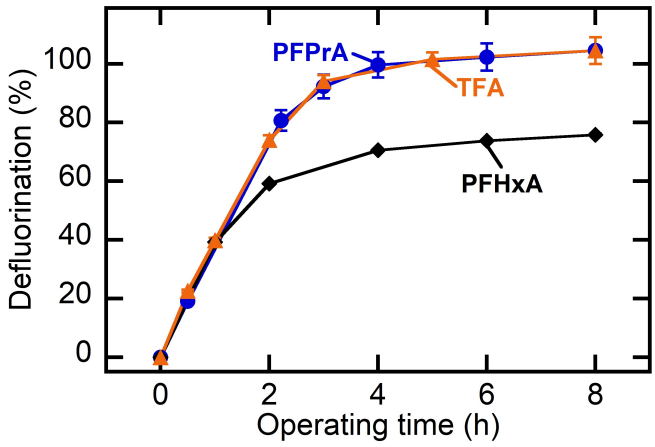

Figure 26. Defluorination kinetics of TFA, PFPrA, and PFHxA for 8 hours of the oxidation process. The figure was generated with two replicates, and the average values along with their standard deviations were plotted.

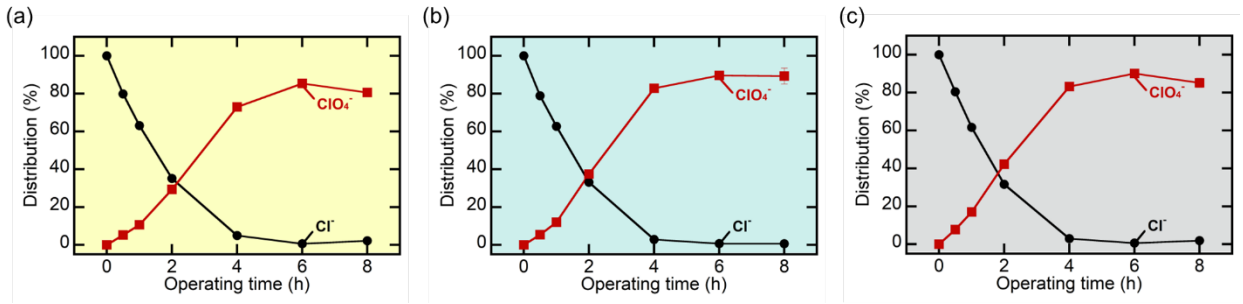

Figure 27. Chloride oxidation kinetics during defluorination of (a) TFA, (b) PFPrA, and (c) PFHxA for 8 hours of the oxidation process. The findings indicate that, on average, 98.4% of Cl^- disappeared, with 85.0% of the initial chloride being converted to ClO_4^-. The remaining chloride (%) and perchlorate production (%) were calculated based on the starting NaCl concentrations (20 mM). The figure was generated with two replicates, and the average values along with their standard deviations were plotted.

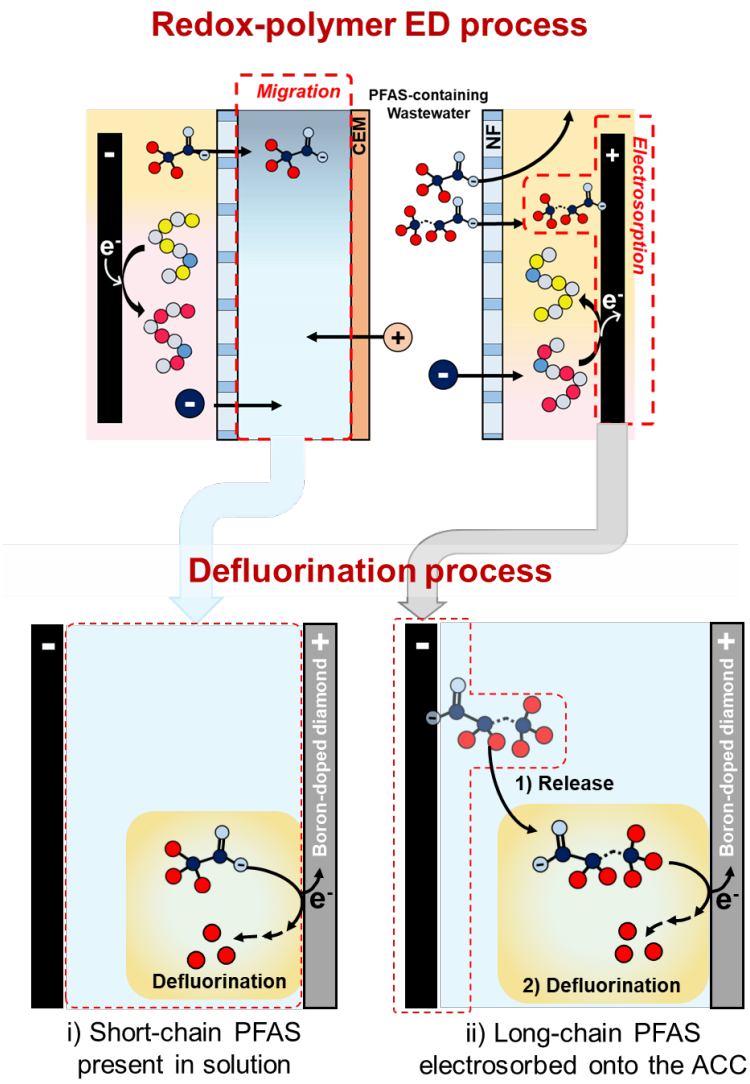

Figure 28. Anticipated defluorination process: i) Defluorination process of short-chain PFAS up-concentrated in solution and ii) long-chain PFAS electrosorbed onto the activated-carbon clothes during the redox-polymer ED process.

SI 7. Supplementary References

1 Björnsdotter, M. K., Yeung, L. W., Kärrman, A. & Jogsten, I. E. Ultra-short-chain perfluoroalkyl acids including trifluoromethane sulfonic acid in water connected to known and suspected point sources in Sweden. *Environmental science & technology* **53**, 11093-11101 (2019).

2 Janda, J., Nödler, K., Brauch, H.-J., Zwiener, C. & Lange, F. T. Robust trace analysis of polar (C2-C8) perfluorinated carboxylic acids by liquid chromatography-tandem mass spectrometry: method development and application to surface water, groundwater and drinking water. *Environmental Science and Pollution Research* **26**, 7326-7336 (2019).

3 Yeung, L. W., Stadey, C. & Mabury, S. A. Simultaneous analysis of perfluoroalkyl and polyfluoroalkyl substances including ultrashort-chain C2 and C3 compounds in rain and river water samples by ultra performance convergence chromatography. *Journal of Chromatography A* **1522**, 78-85 (2017).

4 Freeling, F. & Björnsdotter, M. K. Assessing the environmental occurrence of the anthropogenic contaminant trifluoroacetic acid (TFA). *Current Opinion in Green and Sustainable Chemistry*, 100807 (2023).

5 Scheurer, M. *et al.* Small, mobile, persistent: Trifluoroacetate in the water cycle–Overlooked sources, pathways, and consequences for drinking water supply. *Water research* **126**, 460-471 (2017).

6 Scheurer, M. & Nödler, K. Ultrashort-chain perfluoroalkyl substance trifluoroacetate (TFA) in beer and tea–An unintended aqueous extraction. *Food Chemistry* **351**, 129304 (2021).

7 Sadia, M. *et al.* Occurrence, fate, and related health risks of PFAS in raw and produced drinking water. *Environmental Science & Technology* **57**, 3062-3074 (2023).

8 Jacob, P. & Helbling, D. E. Rapid and Simultaneous Quantification of Short-and Ultrashort-Chain Perfluoroalkyl Substances in Water and Wastewater. *ACS ES&T Water* **3**, 118-128 (2022).

9 Berg, M., Müller, S. R., Mühlemann, J., Wiedmer, A. & Schwarzenbach, R. P. Concentrations and mass fluxes of chloroacetic acids and trifluoroacetic acid in rain and natural waters in Switzerland. *Environmental science & technology* **34**, 2675-2683 (2000).

10 Chen, H. *et al.* Multimedia distribution and transfer of per-and polyfluoroalkyl substances (PFASs) surrounding two fluorochemical manufacturing facilities in Fuxin, China. *Environmental science & technology* **52**, 8263-8271 (2018).

11 Ochoa-Herrera, V. & Sierra-Alvarez, R. Removal of perfluorinated surfactants by sorption onto granular activated carbon, zeolite and sludge. *Chemosphere* **72**, 1588-1593 (2008).

12 Deng, S. *et al.* Enhanced adsorption of perfluorooctane sulfonate and perfluorooctanoate by bamboo-derived granular activated carbon. *Journal of hazardous materials* **282**, 150-157 (2015).

13 Sun, H., Cannon, F. S. & He, X. Enhanced trifluoroacetate removal from groundwater by quaternary nitrogen-grafted granular activated carbon. *Science of the Total Environment* **660**, 577-585 (2019).

14 Baldaguez Medina, P. *et al.* Investigating the Electrochemically Driven Capture and Release of Long-Chain PFAS by Redox Metallopolymer Sorbents. *ACS Applied Materials & Interfaces* **15**, 22112-22122 (2023).

15 Román Santiago, A. *et al.* Imparting Selective Fluorophilic Interactions in Redox Copolymers for the Electrochemically Mediated Capture of Short-Chain Perfluoroalkyl Substances. *Journal of the American Chemical Society* **145**, 9508-9519 (2023).

16 Zhou, J. *et al.* Efficient removal of trifluoroacetic acid from water using surface-modified activated carbon and electro-assisted desorption. *Journal of Hazardous Materials* **436**, 129051 (2022).

17 Du, Z. *et al.* Removal of perfluorinated carboxylates from washing wastewater of perfluorooctanesulfonyl fluoride using activated carbons and resins. *Journal of hazardous materials* **286**, 136-143 (2015).

18 Maimaiti, A. *et al.* Competitive adsorption of perfluoroalkyl substances on anion exchange resins in simulated AFFF-impacted groundwater. *Chemical Engineering Journal* **348**, 494-502 (2018).

19 Zaggia, A., Conte, L., Falletti, L., Fant, M. & Chiorboli, A. Use of strong anion exchange resins for the removal of perfluoroalkylated substances from contaminated drinking water in batch and continuous pilot plants. *Water research* **91**, 137-146 (2016).
20 Li, M. *et al.* Removal mechanisms of perfluorinated compounds (PFCs) by nanofiltration: Roles of membrane-contaminant interactions. *Chemical Engineering Journal* **406**, 126814 (2021).
21 Hang, X., Chen, X., Luo, J., Cao, W. & Wan, Y. Removal and recovery of perfluorooctanoate from wastewater by nanofiltration. *Separation and Purification Technology* **145**, 120-129 (2015).
22 Ma, Q. *et al.* Evaluation of commercial nanofiltration and reverse osmosis membrane filtration to remove per-and polyfluoroalkyl substances (PFAS): Effects of transmembrane pressures and water matrices. *Water Environment Research* **96**, e10983 (2024).